Wave-propagation in rocks saturated by two immiscible fluids

submitted to *Geophys. J. Int.*

Wave-propagation in rocks saturated by two immiscible fluids.

G. Papageorgiou* and M. Chapman†

University of Edinburgh,

Grant Institute, West Mains Road,

Edinburgh EH9 3JW, UK.

SUMMARY

Accurate modelling of the dependence of seismic wave speed from frequency and fluid content is crucial to the quantitative interpretation of seismic data. Dispersive effects such as squirt flow become important at a critical frequency that is proportional to fluid mobility. When a porous medium is partially saturated it is not clear how the respective fluid mobilities are to be averaged. Building on previous work, we use a nonzero, static capillary pressure parameter and a relative permeability model to simulate the effects of squirt flow in a realistic sand saturated by water and CO_2 where the CO_2 can be in either the liquid or supercritical phase. We show that the effective fluid follows a mixing law similar to Brie's empirical model and the effective frequency depends both on the relative permeability model and the capillary pressure parameter which can potentially lead to a dispersive effect in the seismic band.

1 INTRODUCTION

Assessing the impact of partial saturation on seismic waves propagating in porous media is vey important for a variety of applications. For example, CO_2 monitoring of active carbon

capture and storage (CCS) projects relies on accurately estimating the amount and location of CO_2 from seismic surveying.

There is an increasing recognition that the relationship between partial fluid saturation and velocity is more complex than that predicted by the Gassmann-Wood formula, with patchy saturation models gaining in popularity (Eid et al., 2015). Meanwhile, fully saturated rocks are known to exhibit velocity dispersion with a characteristic frequency controlled by fluid mobility (Batzle et al., 2006). The importance of developing a consistent approach which can handle the effects known to be important for both full and partial saturation has been noted by Ghosh et al. (2015).

Papageorgiou & Chapman (2015) developed a model which considered the effects of squirt flow in a rock saturated with two fluids under the assumption that capillary pressure was zero. By contrast, Papageorgiou et al. (2016) studied the effects of capillary pressure on fluid substitution at low frequencies, and showed how "patch-style" effects could be predicted by this approach. The purpose of this paper is to combine these approaches into a consistent model valid over the full range of frequencies and capillary pressures.

Our view is that the patch effect results from systematic variations in the induced pore-pressure between the two fluids, and we capture this effect through a simple model depending on a single non-dimensional parameter. This model then allows us to calculate the squirt-flow behaviour through analysis of the average pressures in the two fluids.

We illustrate the prediction of this new model in the context of the permeable Utsira sand found in the CO_2 storage site of the Sleipner field (Arts et al., 2008). Assuming reservoir conditions, we predict velocity versus saturation for either liquid or supercritical CO_2.

2 ROCK PHYSICS THEORY

A sequence of papers (e.g. Hudson et al., 1996; Chapman et al., 2002; Jakobsen & Chapman, 2009; Papageorgiou & Chapman, 2015) have studied the effect of wave-induced flow on frequency-dependent velocity and attenuation of seismic waves travelling through fluid-saturated rocks. The common approach is to describe the pore space in terms of idealised ellipsoidal inclusions (cracks and pores), which are assumed to have the ability to exchange fluid during the passage of a seismic wave.

Calculation of the velocities and attenuation relies on three major steps. Firstly, an equation of state is developed for each inclusion, relating the fluid mass content, applied stress and fluid pressure. Secondly, an equation is proposed to describe the fluid exchange between inclusions due to differences in fluid pressure. This allows frequency-dependent fluid pressures

to be calculated as a function of applied stress. Finally, equivalent medium theory allows frequency-dependent moduli to be calculated from these induced pressures.

Papageorgiou & Chapman (2015) extended the earlier framework to the case of saturation by two fluids under the assumption that the fluid pressures were constant in each inclusion. In reality, we expect that the induced fluid pressures may differ systematically between the two fluids. Possible reasons for this variation include capillary or membrane effects as well as the influence of uneven spatial variation in the fluid distributions.

This paper further extends the analysis to allow for systematic variations in pressure between the two fluids within each inclusion. We examine the simplest possible model, where the induced fluid pressures in each phase are simply proportional to each other, with the same constant of proportionality in each inclusion. Specifically, we assume a relation between the pressure of fluid 1 P_{g} and pressure P_{w} of fluid 2 that has the form:

$$P_{\mathrm{g}} = qP_{\mathrm{w}}. \tag{1}$$

It should be noted that in what follows, we label the two fluids with indices g, w for readability but our analysis is applicable to *any* two-fluid system, not only water-gas. In what follows we take $K_{\mathrm{g}} < K_{\mathrm{w}}$.

Different values of q could of course be used in different inclusions at the cost of increased algebraic complexity. Although we do not specify the physical mechanism giving rise to the parameter q, we can suggest a range of possible values which may be considered reasonable. Of course, $q = 1$ corresponds to the iso-stress condition applied in Papageorgiou & Chapman (2015). At the other extreme we note that compressing an ideal fluid induces a pressure change which is proportional to the reciprocal of the fluid bulk modulus, and we do not expect induced pressure differences to exceed those in this case. We therefore suggest that q should lie within the limits

$$q_0 < q \leq 1, \qquad \text{where} \qquad q_0 = \frac{K_{\mathrm{g}}}{K_{\mathrm{w}}}. \tag{2}$$

With the definition of equation (1) we are now ready to discuss the equation of state in each inclusion. In the single fluid case, the volume of a crack or pore is given by Chapman et al. (2002):

$$\begin{aligned} \phi^{\ominus} =& \phi_0^{\ominus}\left(1 - \frac{\sigma_{ll}}{3\sigma_c} + \frac{P^{\ominus}}{\sigma_c}\right) \\ \phi^{\odot} =& \phi_0^{\odot}\left(1 - \frac{3}{4\mu}\frac{(1-\nu)}{(1+\nu)}\sigma_{ll} + \frac{3}{4\mu}P^{\odot}\right), \end{aligned} \tag{3}$$

where σ_{ll} is the applied stress, μ is the shear modulus of the grain material and ν its Poisson's

ratio. The compressibility $\frac{1}{\sigma_c}$ depends on the aspect ratio r of the ellipsoid crack:

$$\sigma_c = \frac{\pi \mu r}{2(1-\nu)}, \tag{4}$$

and the pressures $P^{\ominus}$, $P^{\odot}$ refer to the crack and pore average pressure respectively. We adopt the notation convention where superscripts ($P^{\odot}$, $P^{\ominus}$) denote inclusion type (here pore, crack) and subscripts (P_{w}, P_{g}) denote fluid type. In our case, we have two fluid pressures in each inclusion and we intend to calculate the volume change of each inclusion with a weighted average of these pressures. The most general such formula would be of the form:

$$P = \alpha P_{\mathrm{g}} + (1-\alpha) P_{\mathrm{w}}, \qquad \text{where } \alpha = \alpha(S_{\mathrm{w}}) \tag{5}$$

Justifications for the cases $\alpha = 1$ and $\alpha = 0$ could be given for the cases in which only one fluid is in contact with the inclusion surface or when the saturation is uneven between inclusions as we argued in Papageorgiou & Chapman (2015). In a more general scenario, α would be a function of fluid saturation dictated by the wettability of the rock (a recent work where this has been addressed is Glubokovskikh & Gurevich, 2017). Such an assumption would have important implications for the variation of seismic velocity with wettability, an effect that has been recently observed experimentally (see Wang et al., 2015)

Nevertheless we postpone such a discussion for future work and choose to weigh the pressures with the saturation ($\alpha = S_{\mathrm{w}}$) in the current work. In doing this, we assume that the saturations are equal in each inclusion type. We therefore write

$$\begin{aligned} P^{\ominus} =& S_{\mathrm{w}} P_{\mathrm{w}}^{\ominus} + (1-S_{\mathrm{w}}) P_{\mathrm{g}}^{\ominus} = \widetilde{q}\, P_{\mathrm{w}}^{\ominus} \\ P^{\odot} =& S_{\mathrm{w}} P_{\mathrm{w}}^{\odot} + (1-S_{\mathrm{w}}) P_{\mathrm{g}}^{\odot} = \widetilde{q}\, P_{\mathrm{w}}^{\odot} \end{aligned} \tag{6}$$

where $\widetilde{q} = S_{\mathrm{w}} + q(1-S_{\mathrm{w}})$ and in the second equation we have used the definition (1).

The density ρ_f of each fluid varies from its undisturbed value $\rho_f^{(0)}$ in a way that depends on pressure variations P_f via the formula:

$$\rho_f = \frac{\rho_f^{(0)}}{1 - \frac{P_f}{K_f}} \simeq \rho_f^{(0)} \left(1 + \frac{P_f}{K_f}\right), \tag{7}$$

where $1/K_f$ is the fluid compressibility. This allows us to relate fluid mass content m, fluid pressure and applied stress through equations (3), (6), (7):

$$\begin{aligned} m_{\mathrm{w}}^{\ominus} =& S_{\mathrm{w}}\, \rho_{\mathrm{w}}^{\ominus} \phi^{\ominus} & m_{\mathrm{w}}^{\odot} =& S_{\mathrm{w}}\, \rho_{\mathrm{w}}^{\odot} \phi^{\odot} \\ m_{\mathrm{g}}^{\ominus} =& (1-S_{\mathrm{w}})\, \rho_{\mathrm{g}}^{\ominus} \phi^{\ominus} & m_{\mathrm{w}}^{\odot} =& (1-S_{\mathrm{w}})\, \rho_{\mathrm{g}}^{\odot} \phi^{\odot}, \end{aligned} \tag{8}$$

In Chapman et al. (2002), mass exchange between inclusions was described by the following formula:

$$\partial_t m^{\odot} = \frac{\rho^{(0)}}{g}(P^{\ominus} - P^{\odot}) = -\partial_t m^{\ominus} \tag{9}$$

in which the coefficient g is given as

$$\frac{1}{g} = l\frac{k}{\eta}. \tag{10}$$

where l is a characteristic length scale and $\frac{k}{\eta}$ is the fluid mobility: the ratio of rock permeability to fluid dynamic viscosity.

Equation (9) is based ultimately on Darcy's law which states that the fluid flux $\partial_t Q$ (representing fluid volume per unit time) in a porous medium of cross-sectional area A is proportional to the pressure gradient $\partial_x P$ driving the flux along direction x. The constant of proportionality is the fluid mobility :

$$\partial_t Q = -A\frac{k}{\eta}\partial_x P. \tag{11}$$

In multi-fluid Darcy's law it is assumed that the volume flux of each fluid $Q_{\rm w}, Q_{\rm g}$ is proportional to the pressure gradient of each fluid's pressure along x but the constant of proportionality is scaled down by the relative permeability:

$$\begin{aligned} \partial_t Q_{\rm w} &= -A\frac{k}{\eta_{\rm w}}k_{\rm w}\partial_x P_{\rm w} \\ \partial_t Q_{\rm g} &= -A\frac{k}{\eta_{\rm g}}k_{\rm g}\partial_x P_{\rm g}. \end{aligned} \tag{12}$$

Here, the relative permeabilities $k_{\rm w}, k_{\rm g}$ are such that $0 \leq k_{\rm w} + k_{\rm g} \leq 1$ (see, for example Brooks & Corey, 1964; Myron III et al., 2013) and $\eta_{\rm w}, \eta_{\rm g}$ are the dynamic viscosities of the fluids.

Chapman et al. (2002) approximate equation (11) to first order by assuming $\partial_x P \simeq \frac{P_2 - P_1}{l}$ and $A \simeq l^2$ where l is a length scale characteristic of the pore network and P_2, P_1 fluid pressures at neighbouring pores. They also approximate the mass flux using the undisturbed fluid density $\rho^{(0)}$ by $\partial_t m \simeq \rho^{(0)}\partial_t Q$. By analogy to the multi-fluid Darcy's law of equation (12), we therefore describe multi-fluid flow in the pore network by the equations:

$$\begin{aligned} \partial_t m_{\rm w}^{\ominus} &= \frac{\rho_{\rm w}^{(0)}}{g_{\rm w}}\,(P_{\rm w}^{\odot} - P_{\rm w}^{\ominus}) = -\partial_t m_{\rm w}^{\odot} \\ \partial_t m_{\rm g}^{\ominus} &= \frac{\rho_{\rm g}^{(0)}}{g_{\rm g}}\,(P_{\rm g}^{\odot} - P_{\rm g}^{\ominus}) = -\partial_t m_{\rm g}^{\odot}, \end{aligned} \tag{13}$$

where now

$$\frac{1}{g_{\rm w}} = lk\frac{k_{\rm w}}{\eta_{\rm w}} \qquad \frac{1}{g_{\rm g}} = lk\frac{k_{\rm g}}{\eta_{\rm g}}. \tag{14}$$

Combining equations (8),(13) and keeping only first order terms in the pressures and stresses we arrive at the following system of equations for the dynamics of volume-averaged

pressures $P^{\odot}, P^{\ominus}$:

$$\begin{aligned} \frac{3\phi_0^{\odot}}{4\mu}\partial_t\left[(1+K_p)\,P^{\odot}-\frac{1-\nu}{1+\nu}\sigma_{ll}\right] &= \frac{1}{g}(P^{\ominus}-P^{\odot}) \\ \frac{\phi_0^{\ominus}}{\sigma_c}\partial_t\left[(1+K_c)\,P^{\ominus}-\frac{\sigma_{ll}}{3}\right] &= \frac{1}{g}(P^{\odot}-P^{\ominus}) \end{aligned} \tag{15}$$

where the quantity $1/g$ is depends on q and the multi-fluid Darcy constants of equation (14):

$$\frac{1}{g} = \frac{1}{\widetilde{q}}\left(\frac{1}{g_{\mathrm{w}}}+q\frac{1}{g_{\mathrm{g}}}\right) \tag{16}$$

Equation (15) can be solved in the frequency domain, yielding the solutions:

$$\begin{aligned} P^{\ominus} &= A(\omega)\sigma_{ii} \\ P^{\odot} &= B(\omega)\sigma_{ii}, \end{aligned} \tag{17}$$

where, in analogy with Chapman (2003), we have defined the following dimensionless parameters:

$$\begin{aligned} A(\omega) &= \frac{\frac{1+\mathrm{i}\omega\gamma\tau_m}{3(1+K_c)}+\gamma'}{1+(1+\mathrm{i}\omega\tau_m)\gamma} & B(\omega) &= \frac{\frac{1}{3(1+K_c)}+(1+\mathrm{i}\omega\tau_m)\gamma'}{1+(1+\mathrm{i}\omega\tau_m)\gamma} \\ K_p &= \frac{4\mu}{3K_f} & K_c &= \frac{\sigma_c}{K_f} \\ \gamma &= \frac{3\phi_0^{\odot}\sigma_c(1+K_p)}{4\phi_0^{\ominus}\mu(1+K_c)} & \gamma' &= \gamma\frac{1-\nu}{(1+\nu)(1+K_p)}. \end{aligned} \tag{18}$$

The effective fluid compressibility and effective time scale parameter depend on both fluids in a way that involves the parameter q. Explicitly:

$$\frac{1}{K_f} = \frac{1}{\tilde{q}}\left(\frac{S_{\mathrm{w}}}{K_{\mathrm{w}}}+q\frac{(1-S_{\mathrm{w}})}{K_{\mathrm{g}}}\right) \qquad \frac{1}{\tau_m} = \frac{\sigma_c\ k\ l}{\phi_0^{\ominus}(1+K_c)}\ \frac{1}{\tilde{q}}\left(\frac{k_{\mathrm{w}}}{\eta_{\mathrm{w}}}+\frac{qk_{\mathrm{g}}}{\eta_{\mathrm{g}}}\right). \tag{19}$$

To distinguish between the impact of rock and fluid properties in τ_m we write

$$\frac{1}{\tau_m} = \frac{P_0}{(1+K_c)\widetilde{q}}\left(\frac{k_{\mathrm{w}}}{\eta_{\mathrm{w}}}+q\frac{k_{\mathrm{g}}}{\eta_{\mathrm{g}}}\right) \tag{20}$$

Where P_0 a scaling parameter with dimensions Pa incorporating the unknowns relevant to rock properties. The contribution of the dimensionless quantity K_c can be ignored if $\sigma_c \ll K_f$ but as K_f depends on fluid saturation, we need to ensure that the aspect ratio is small enough to warrant the assumption $\sigma_c \ll K_f$ if K_c is to be ignored.

As a final step, we use equivalent medium theory to calculate the frequency dependent moduli from the pressures induced by fluid exchange in the inclusions. Chapman (2003) gave an expression for the frequency-dependent bulk modulus in the single fluid case which can be written in a form directly applicable to the effective fluid defined by equation (19):

$$K_{\mathrm{eff.}}(\omega) = K_{\mathrm{dry}} + \phi_0^{\ominus}\left(1+\frac{K_{\mathrm{m}}}{\sigma_c}\right)K_m\frac{P^{\ominus}}{\sigma_{ii}} + \phi_0^{\odot}\left(1+\frac{3K_{\mathrm{m}}}{4\mu}\right)K_m\frac{P^{\odot}}{\sigma_{ii}}. \tag{21}$$

Using our averaged pressure solution in each crack and pore from equation (17), the coefficients $A(\omega), B(\omega)$ can be readily inserted in equation (21), to obtain

$$K_{\text{eff.}}(\omega) = K_{\text{dry}} + \phi_0^{\ominus} \left(1 + \frac{K_{\text{m}}}{\sigma_c}\right) K_{\text{m}}\, A(\omega) + \phi_0^{\odot} \left(1 + \frac{3K_{\text{m}}}{4\mu}\right) K_{\text{m}}\, B(\omega), \tag{22}$$

where the dried modulus K_{dry} is defined as

$$K_{\text{dry}} = K_m - K_m^2 \left(\frac{9\phi_0^{\odot}}{4\mu}\frac{1-\nu}{1+\nu} + \frac{\phi_0^{\ominus}}{\sigma_c}\right). \tag{23}$$

3 MODELLING A DISPERSIVE CO_2 SAND

To show the potential impact of this theory on a realistic setting we choose a well-studied CO_2 storage reservoir: the Sleipner field. The Sleipner field consists of a layered structure of nine sand layers separated by thin shales called the Utsira formation. The formation itself is encased between thicker shale layers and because of the extent of previous studies on the site (for example Arts et al., 2004; Carcione et al., 2006; Rubino et al., 2011; Ghosh et al., 2015) and extensive monitoring time-lapse surveys, the lithologies of the Utsira formation are estimated with relative accuracy.

Here we focus our effort in modelling the Utsira sand using the squirt-flow model described in Section 2. The capillary pressure parameter q defined via equation (3) is kept a tuning parameter. It was shown in Papageorgiou et al. (2016) that the theoretically derived effective fluid modulus in equation (19) resembles the empirical mixing law of Brie et al. (1995):

$$K_f = (K_{\text{w}} - K_{\text{g}})S_{\text{w}}^e + K_{\text{g}}, \qquad 1 \le e \le 40 \tag{24}$$

when $q = e^{\frac{2}{3}}$. Brie's law has been used extensively to account for patchy saturation in the CO_2 literature in both field (Perozzi et al., 2016; Eid et al., 2015; Grude et al., 2014; Azuma et al., 2011; Lumley, 2010; Carcione et al., 2006) and lab data (Kim et al., 2011).

In the current context there is no association between the parameter q and the concept of a saturation patch, or at least not in a way that involves a characteristic length for that patch. Instead, q quantifies the variation of capillary pressure C since $\Delta C = (q-1)\Delta P_{\text{w}}$. In Section 2 we showed that the effective fluid mobility of equation (10) is an average weighted by q. This means that, in a partially saturated attenuative target, the parameter q also affects the spectral profile of the reflection as well as the stiffness of the effective fluid.

To demonstrate this, let us calculate the relaxation time of the Utsira sand. A relative permeability model and an appropriate scaling is needed as per equation (20). For a relative permeability model we choose the generic form shown in Figure 1. The (rock-dependent)

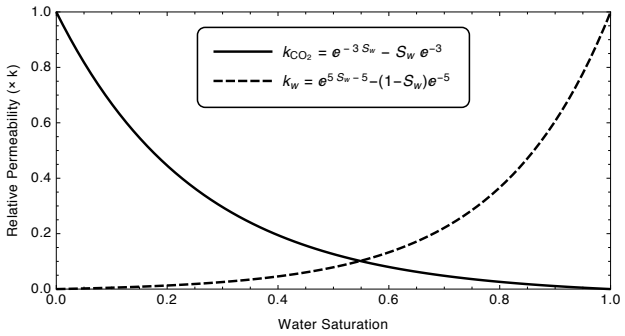

Figure 1. Relative permeability model for a reservoir saturated by CO_2 and water.

scaling constant P_0 of equation (20) is not easily calculated so we use an arbitrary scaling by setting the water-saturated value of the timescale parameter $\omega_0(S_w = 1) = \frac{2\pi}{\tau_m} = 1$ and examining the partially saturated behaviour of the characteristic time-scale relative to this value.

We note that at full water saturation, the value $\tau_m \sim 10^{-5}$ sec has been used for example in Chapman (2003); Ghosh et al. (2015). In terms of the fluid content, the behaviour of the characteristic frequency and elastic behaviour of the sand at intermediate saturations depends on the phase of the saturating CO_2. Liquid CO_2 is stiff, dense and more viscous than the much softer and more dilute supercritical CO_2. Even though almost always the injected CO_2 is supercritical, both states are physically plausible in reservoir conditions.

To determine the impact of each state on the rock physics, we read the fluid properties of CO_2 at an overburden pressure of 8 MPa (beyond the critical pressure) and at 28°C and 45°C corresponding respectively to liquid and super-critical CO_2. The properties are taken from the Wolfram|Alpha and NIST databases. The viscosity, fluid moduli and density for each chosen temperature are shown in Table 2.

The non-dimensional characteristic frequency and its dependency on the capillary pressure parameter q is shown in Figure 2 for liquid, and in Figure 3 for supercritical CO_2. It is evident from these figures that the relative permeability effect can result in a squirt flow frequency lower than the fully water saturated value and this effect is amplified depending on the value of the parameter q. In the squirt-flow theory presented here this would imply that the effect of patches manifests itself in a lowering of the characteristic frequency as well as a stiffening the effective fluid in intermediate saturations.

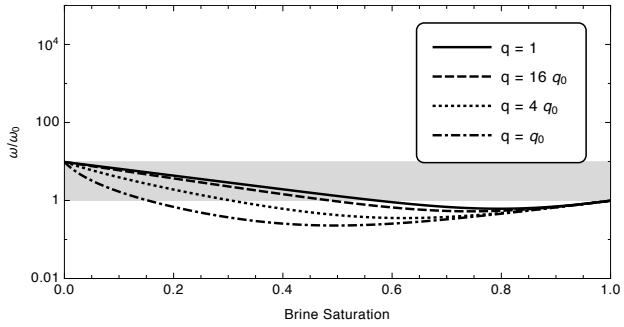

Figure 2. Scaled characteristic frequency for liquid CO_2 below the critical temperature at 8 MPa. The frequency scaling is set to 1 at the water saturation end and the range of relative mobilities for CO_2/Brine is coloured grey.

4 RESULTS

Using the effective time-scale of equation (20) in the frequency-dependent bulk modulus $K_{\text{eff}}(\omega)$ of equation (22) the Utsira sand can be modelled using the parameters in Table 1. In fact, a more illuminating formula can be derived if we partition the effective modulus of equation (22) to its low and high frequency limits:

$$K_{\text{eff}}(\omega) = K_d + K_m \frac{\left[1+3\left(1+K_c\right)\gamma'\right]\left[\phi_0^{\ominus}\left(1+\frac{K_m}{\sigma_c}\right)+\phi_0^{\odot}\left(1+\frac{3K_m}{4\mu}\right)\right]}{\left(\gamma+1\right)\left(1+K_c\right)} + K_m \frac{\left[\gamma-3\left(1+K_c\right)\gamma'\right]\left[\gamma\phi_0^{\ominus}\left(1+\frac{K_m}{\sigma_c}\right)-\phi_0^{\odot}\left(1+\frac{3K_m}{4\mu}\right)\right]}{\gamma(\gamma+1)\left(1+K_c\right)\left(1-i\frac{\gamma+1}{\gamma\omega\tau}\right)} \tag{25}$$

Although it is not entirely straightforward to see, the first two terms of the right hand side of this equation are Gassmann's formula as was noted in Chapman et al. (2002). The other term, is a Maxwell element and the model is a standard linear solid, a fact that has been observed

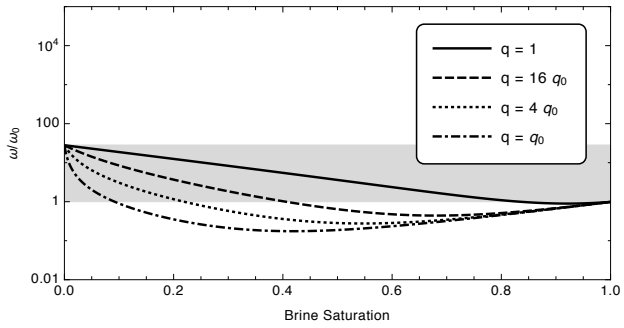

Figure 3. Scaled characteristic frequency for super-critical CO_2 at 8 MPa. The frequency scaling is set to 1 at the water saturation end and the range of relative mobilities for CO_2/Brine is coloured grey.

Utsira sand properties	
porosity ϕ_0:	37.5%
crack dens. ϵ:	1.0×10^{-2}
asp. ratio r:	1.0×10^{-4}
intrinsic perm. k (m^2):	1.0×10^{-11}
dry frame modulus (Pa):	1.4×10^9
shear frame modulus (Pa):	2.0×10^9
mineral modulus (Pa):	4.2×10^{10}
shear mineral modulus (Pa):	2.1×10^{10}
solid density (Kg/m^3):	2650

Table 1. Parameters used to model Utsira sand.

before by Hao & He (2013). This is an important observation since the standard linear solid model has been experimentally verified against partial saturation, frequency-dependent data obtained in the laboratory (Chapman et al., 2017). It is now trivial to expand equation (25) in a real and complex part so we can write

$$\frac{\rho}{K_{\text{eff}}(\omega) + \frac{4}{3}\mu} = \frac{1}{V_p^2} + \mathrm{i}\frac{1}{QV_p^2} \qquad \text{with} \qquad Q, V_p > 0. \tag{26}$$

Note that both p-wave velocity V_p and attenuation $1/Q$ depend on frequency, water saturation and the parameter q. The dependence is a complicated one as q affects the characteristic frequency and thus the strength of the squirt-flow effect at different water saturation. This is contrary to modelling approaches used thus far where the fluid mixing law enters the model in an ad-hoc way and the impacts of this on the characteristic frequency are either ignored or superimposed in the case of a dispersive effective fluid (i.e. Ghosh et al., 2015).

Explicitly, the behaviour of velocity and attenuation with saturation is shown in Figures 4, 5, 6 for different relative frequency values.

	CO_2 (liq.)	CO_2 (s/crit.)	Brine
temperature (°C):	28	45	N/A (avg)
modulus (Pa):	7.9×10^7	1.1×10^7	2.4×10^9
viscosity (Pa.s):	6.1×10^{-5}	2.1×10^{-5}	6.0×10^{-4}
density (Kg/m^3):	740	240	1000

Table 2. Parameters used to model fluids.

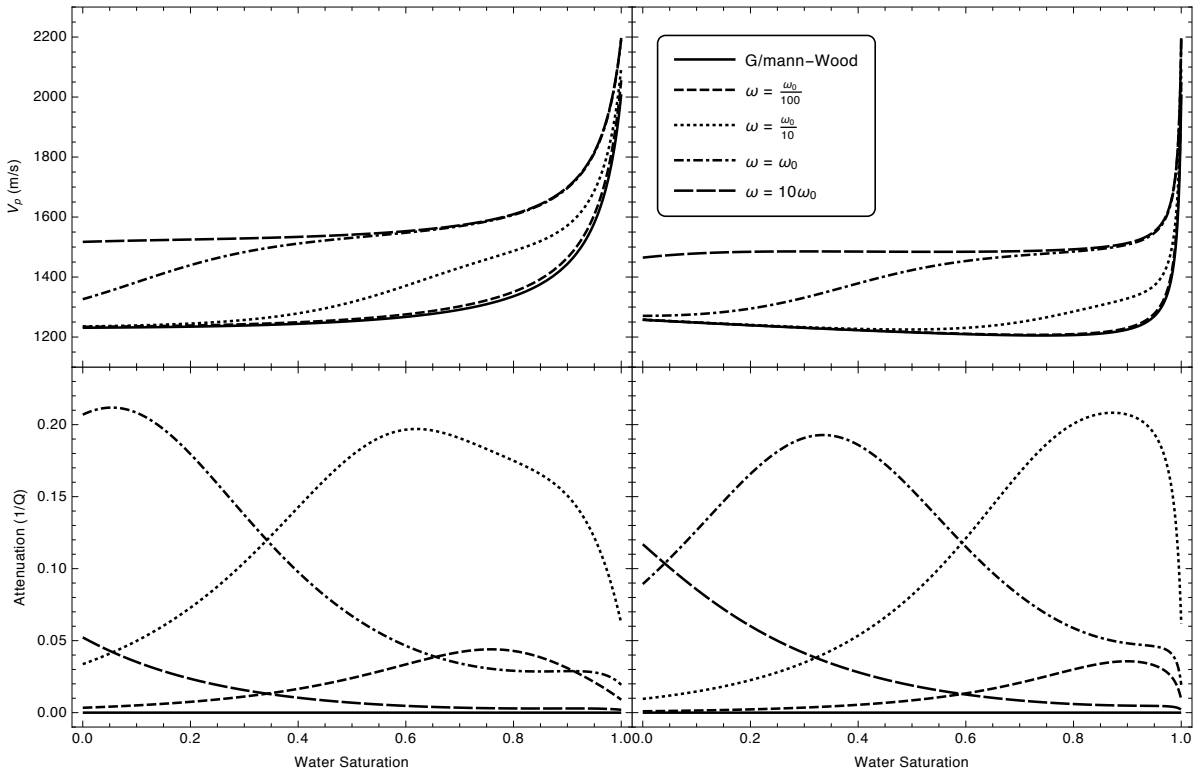

Figure 4. The variation of p-wave velocity and attenuation with water saturation for a partially saturated liquid(left) and supercritical(right) CO_2 sand for different relative frequencies. The capillary pressure parameter is set to 1 and the model reduces to the Gassmann-Wood model at low frequencies.

5 DISCUSSION

The use of the Gassman-Wood technique has traditionally been the most popular method for performing fluid substitution for mixed fluid saturation. This theory follows from an isostress assumption which states that the fluid pressure cannot vary either between fluids or spatially within the pore space.

It has been established that a lack of spatial variation in fluid pressure requires fluid mobility to relax pressure gradients, leading to a frequency-dependent process often referred to as squirt dispersion. But there are many reasons why the fluid pressure should also cary between the fluids. Surface energy and membrane stress considerations will usually ensure that the fluid pressures cannot be equalised, and "patch" effects may mean that the fluids do not effectively communicate with each other. We expect such effects to be non-trivial related to the pore-scale distribution of the fluids.

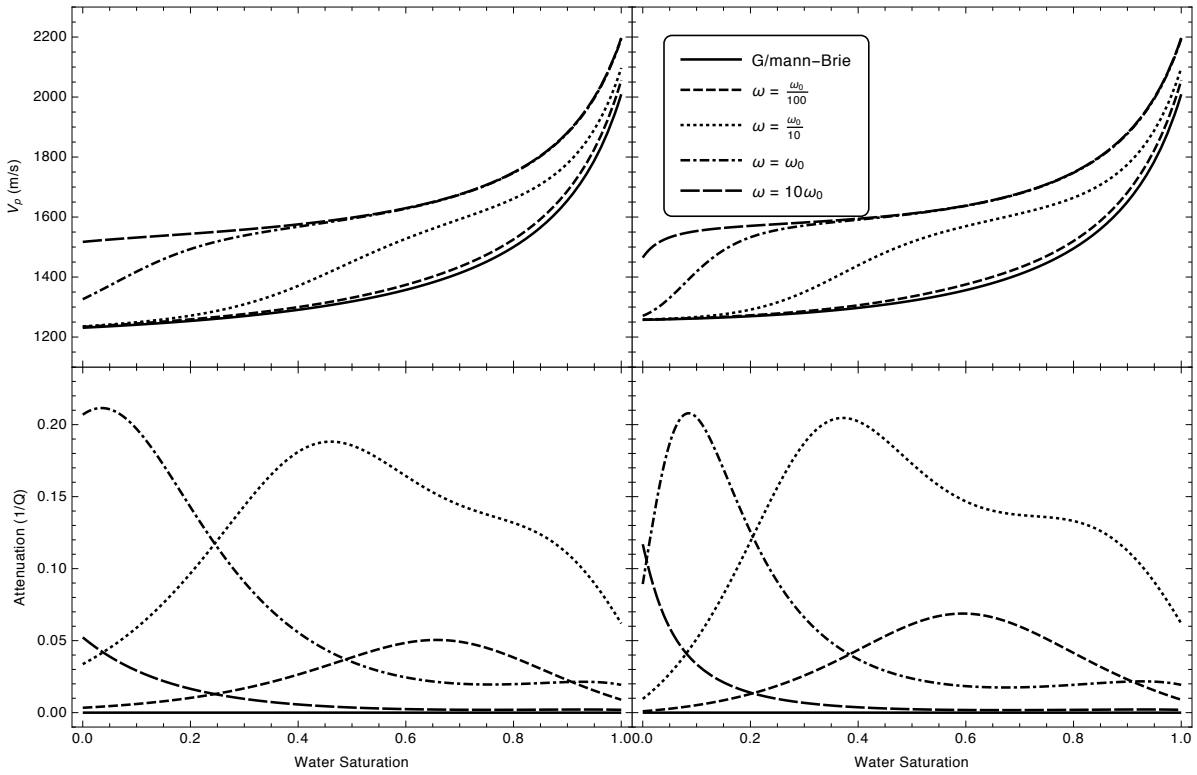

Figure 5. The variation of p-wave velocity and attenuation with water saturation for a partially saturated liquid(left) and supercritical(right) CO_2 sand for different relative frequencies. The capillary pressure parameter is set to $10\frac{K_{CO_2}}{K_w}$ and the model reduces to Gassmann's model with the effective fluid of equation (19) (referred to as Gassmann-Brie model) at low frequencies.

We account for these inter-fluid effects through the introduction of a new non-dimensional parameter and, while we offer no explicit modelling of its dependencies, we argue physically that it must lie between one and the ratio of the fluid bulk moduli. The novelty of our work is then to describe wave propagation through a system in which both squirt flow and the inter-fluid effects are present.

Our model contains previously published work as appropriate limits. As q tends to 1, we recover the multi-fluid squirt flow model of Papageorgiou & Chapman (2015), while as frequency tends to zero we obtain the "Brie like" fluid mixing law of Papageorgiou et al. (2016) The dependencies are represented schematically in Figure 7. Practical application of the work would require estimating both the characteristic frequency scaling and the value for q. The effect of these parameters is coupled in the intermediate saturation and frequency ranges but not at the limits.

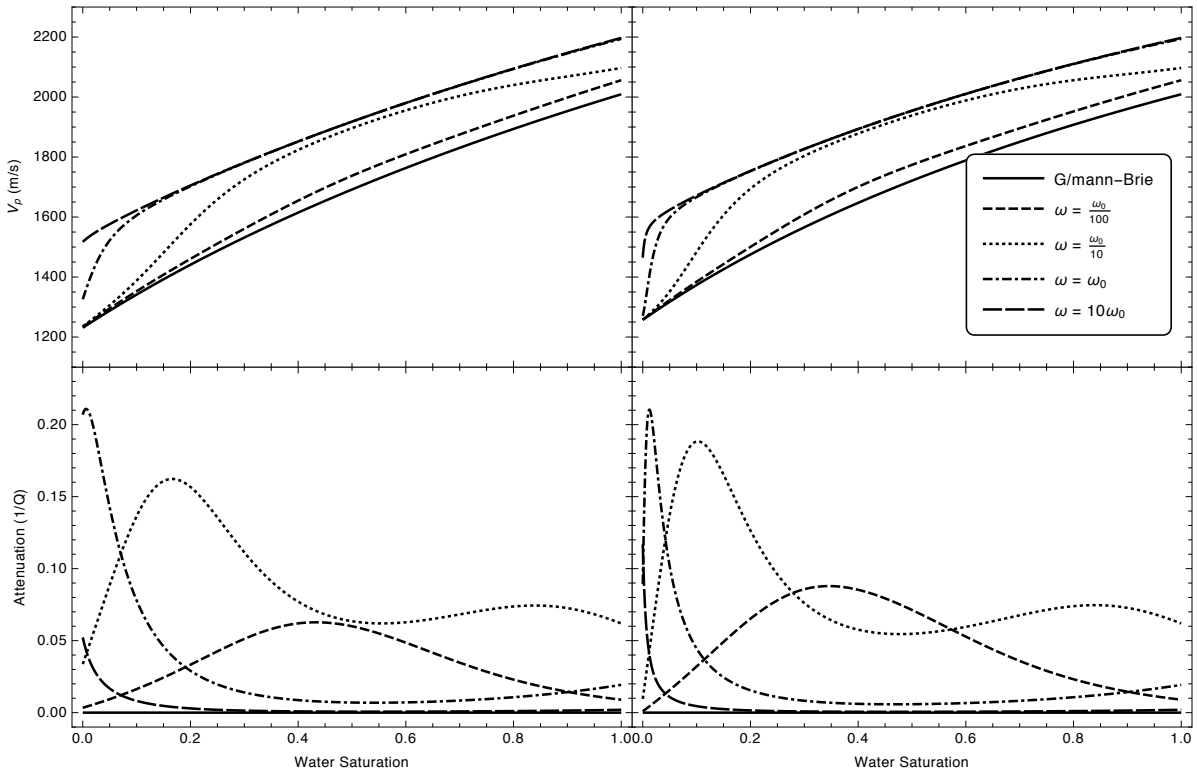

Figure 6. The variation of p-wave velocity and attenuation with water saturation for a partially saturated liquid(left) and supercritical(right) CO_2 sand for different relative frequencies. The capillary pressure parameter is set to the extreme value $\frac{K_{CO_2}}{K_w}$ and the model reduces to Gassmann's model with an arithmetic averaged fluid mixing law (referred to as Gassmann-Brie model) at the low frequency limit.

There are several features of the model we presented here that are important and distinctive. Our characteristic frequency depends on the relative permeability, and as a consequence may be lower for intermediate saturations than in either of the single saturation limits. The behaviour with respect to changing saturation often resembles that of a patch based model, but there is no patch size or characteristic frequency associated to this effect. This suggests that the interpretation of seismic data in terms of a "patch size" parameter may well be ambiguous.

Many of these features are evident in the Utsira sand example for a CO_2-water mixture: the relative permeability effect was shown to reduce the characteristic frequency significantly lower than its water-saturated value. Furthermore, for certain values of the parameter q we observe two peaks in the attenuation for different CO_2 saturations.

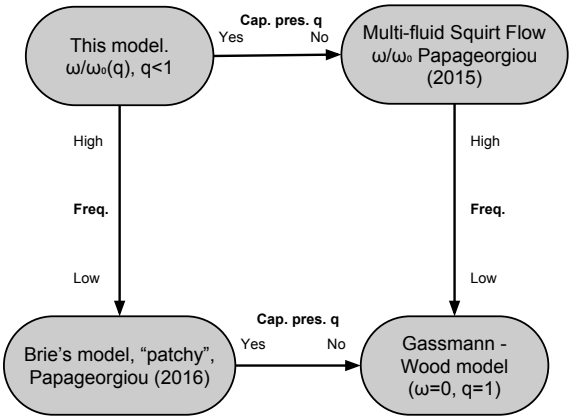

Figure 7. The rock physics model presented here and its relation to previous work. The characteristic frequency of the model is dependent on the parameter q for partial saturation scenaria. When $q = 1, \omega = 0$ this model reduces to the Gassmann-Wood equation.

6 CONCLUSIONS

We have presented an extension to the model of Papageorgiou & Chapman (2015) that includes the effects of capillary pressure which enters the model as a non-dimensional parameter q. We have shown that this parameter affects both the stiffness and the mobility of the effective fluid and we have presented a simple formulation of this model as a standard linear solid that is appropriate for practical applications. Our results demonstrate that, in partial saturation scenaria, the characteristic squirt frequency may be lower than that dictated by the mobility of the more viscous fluid if the relative permeability effect is taken into account. By applying our results to an example drawn from CO_2 storage we assessed the impacts of the above modelling approach in the velocity and attenuation of a sand of a saline aquifer, partially saturated by either liquid or supercritical CO_2.

7 ACKNOWLEDGMENTS

This work was carried out within the DiSECCS project `https://www.bgs.ac.uk/diseccs` (EP/K035878/1). DISECCS is funded by the Engineering and Physical Sciences Research Council (EPSRC) UK.

REFERENCES

Arts, R., Eiken, O., Chadwick, A., Zweigel, P., Van der Meer, L., & Zinszner, B., 2004. Monitoring of co$_2$ injected at sleipner using time-lapse seismic data, *Energy*, **29**(9), 1383–

1392.

Arts, R., Chadwick, A., Eiken, O., Thibeau, S., & Nooner, S., 2008. Ten years' experience of monitoring co2 injection in the utsira sand at sleipner, offshore norway, *First break*, **26**(1).

Azuma, H., Konishi, C., Nobuoka, D., Xue, Z., & Watanabe, J., 2011. Quantitative co 2 saturation estimation from time lapse sonic logs by consideration of uniform and patchy saturation, *Energy Procedia*, **4**, 3472–3477.

Batzle, M. L., Han, D.-H., & Hofmann, R., 2006. Fluid mobility and frequency-dependent seismic velocitydirect measurements, *Geophysics*, **71**(1), N1–N9.

Brie, A., Pampuri, F., Marsala, A., Meazza, O., et al., 1995. Shear sonic interpretation in gas-bearing sands, in *SPE Annual Technical Conference*, vol. 30595, pp. 701–710.

Brooks, R. & Corey, A., 1964. Hydraulics properties of porous media, colorado state univ, *Hydrol. Paper*, (3).

Carcione, J. M., Picotti, S., Gei, D., & Rossi, G., 2006. Physics and seismic modeling for monitoring co2 storage, *Pure and Applied Geophysics*, **163**(1), 175–207.

Chapman, M., 2003. Frequency-dependent anisotropy due to meso-scale fractures in the presence of equant porosity, *Geophysical Prospecting*, **51**(5), 369–379.

Chapman, M., Zatsepin, S. V., & Crampin, S., 2002. Derivation of a microstructural poroelastic model, *Geoph. Jour. Int.*, **151**(2), 427–451.

Chapman, S., Quintal, B., Tisato, N., & Holliger, K., 2017. Frequency scaling of seismic attenuation in rocks saturated with two fluid phases, *Geophysical Journal International*, **208**(1), 221–225.

Eid, R., Ziolkowski, A., Naylor, M., & Pickup, G., 2015. Seismic monitoring of co 2 plume growth, evolution and migration in a heterogeneous reservoir: Role, impact and importance of patchy saturation, *International Journal of Greenhouse Gas Control*, **43**, 70–81.

Ghosh, R., Sen, M. K., & Vedanti, N., 2015. Quantitative interpretation of co 2 plume from sleipner (north sea), using post-stack inversion and rock physics modeling, *International Journal of Greenhouse Gas Control*, **32**, 147–158.

Glubokovskikh, S. & Gurevich, B., 2017. Effect of grain-scale gas patches on the seismic properties of double porosity rocks, *Geophysical Journal International*, **208**(1), 432–436.

Grude, S., Landrø, M., White, J., & Torsæter, O., 2014. Co_2 saturation and thickness predictions in the tubåen fm., snøhvit field, from analytical solution and time-lapse seismic data, *International Journal of Greenhouse Gas Control*, **29**, 248–255.

Hao, Q. & He, Q., 2013. A standard linear solid model representation of frequency-dependent anisotropy due to multiple sets of aligned meso-scale fractures, *Journal of Seismic Explo-*

ration, **22**(2), 169–182.

Hudson, J., Liu, E., & Crampin, S., 1996. The mechanical properties of materials with interconnected cracks and pores, *Geophysical Journal International*, **124**(1), 105–112.

Jakobsen, M. & Chapman, M., 2009. Unified theory of global flow and squirt flow in cracked porous media, *Geophysics*, **74**(2), WA65–WA76.

Kim, J., Matsuoka, T., & Xue, Z., 2011. Monitoring and detecting co2 injected into water-saturated sandstone with joint seismic and resistivity measurements, *Exploration Geophysics*, **42**(1), 58–68.

Lumley, D., 2010. 4d seismic monitoring of co 2 sequestration, *The Leading Edge*, **29**(2), 150–155.

Myron III, B., Behie, G. A., & Trangenstein, J. A., 2013. *Multiphase Flow in Porous Media: Mechanics, Mathematics, and Numerics*, vol. 34, Springer Science & Business Media.

Papageorgiou, G. & Chapman, M., 2015. Multifluid squirt flow and hysteresis effects on the bulk modulus–water saturation relationship, *Geophysical Journal International*, **203**(2), 814–817.

Papageorgiou, G., Amalokwu, K., & Chapman, M., 2016. Theoretical derivation of a brie-like fluid mixing law, *Geophysical Prospecting*.

Perozzi, L., Gloaguen, E., Giroux, B., & Holliger, K., 2016. A stochastic inversion workflow for monitoring the distribution of co2 injected into deep saline aquifers, *Computational Geosciences*, pp. 1–14.

Rubino, J. G., Velis, D. R., & Sacchi, M. D., 2011. Numerical analysis of wave-induced fluid flow effects on seismic data: Application to monitoring of co2 storage at the sleipner field, *Journal of Geophysical Research: Solid Earth*, **116**(B3).

Wang, Z., Schmitt, D. R., & Wang, R., 2015. Does wettability influence seismic wave propagation in liquid-saturated porous rocks?, *Geophysical Journal International*, **203**(3), 2182–2188.